Pergamon

J. Quant. Spectrosc. Radiat. Transfer Vol. 54, No. 5, pp. 837–850, 1995
Elsevier Science Ltd. Printed in Great Britain

0022-4073(95)00105-0

COLLISIONAL SHIFT AND BROADENING OF IODINE SPECTRAL LINES IN AIR NEAR 543 nm

D. G. FLETCHER† and J. C. McDANIEL‡

†NASA Ames Research Center, MS229-1, Moffett Field, CA 94035-1000, U.S.A. and ‡Aerospace Research Laboratory, University of Virginia, Charlottesville, VA 22903, U.S.A.

(Received 21 November 1994)

Abstract—The collisional processes that influence the absorption of monochromatic light by iodine in air have been investigated. Measurements were made in both a static cell and an underexpanded jet flow over the range of properties encountered in typical compressible-flow aerodynamic applications. Experimentally measured values of the collisional shift and broadening coefficients were 0.058 ± 0.004 and 0.53 ± 0.010 GHz $K^{0.7}$/torr, respectively. The measured shift value showed reasonable agreement with theoretical calculations based on Lindholm–Foley collisional theory for a simple dispersive potential. The measured collisional broadening showed less favorable agreement with the calculated value.

INTRODUCTION

In recent years, a variety of Laser-Induced Fluorescence (LIF) techniques have been developed to provide measurements of gasdynamic properties in aerodynamic applications.[1] These laser-based diagnostics are minimally intrusive and they provide flow information at the molecular level with high spatial resolution. Most of the LIF techniques rely on a numerical model of the fluorescence process to infer the thermodynamic properties of the flow from the influence of collisions on the absorption and/or emission of monochromatic light. Accurate measurement of the thermodynamic properties therefore requires a thorough knowledge of the strength and scaling of the collisional dynamics. This, in turn, requires experimental measurements of the important collisional processes at conditions that are similar to those of the intended application.[2,3]

Laser-Induced Iodine Fluorescence (LIIF) is one example of an LIF technique that has been extensively developed to provide measurements of local thermodynamic properties, as well as velocities, in air and nitrogen flows.[4–11] More recently, the strong absorption spectrum of iodine has been exploited as a sharp cutoff filter for Doppler-shifted Mie- and Rayleigh-scattering based velocity measurements.[12–14] Both of these applications rely on a numerical model of the absorption process that must include an accurate representation of the collisional effects.

This report summarizes an experimental investigation of the collisional processes that influence the absorption of light by iodine seeded in air. After a brief theoretical discussion of collisional shift and broadening for I_2 in air, the experimental measurements are presented for the static-cell and jet-flow studies. Finally, the collisional shift and broadening measurements from both experiments are compared with approximate calculations from collisional theory.

COLLISIONAL SHIFT AND BROADENING THEORY

The collisional shift and broadening of molecular absorption transitions result from collisions between the optically active molecules and their perturbers.[15,16] These collisions between molecules cause a shift in their energy levels, which alters the width and location of spectral lines. The magnitude of the energy level shift depends on the electronic configurations of the molecules involved and their relative speed and separation distance during the collision. Because interstellar

radiation is also influenced by the collisional shift and broadening of spectral lines, this field received considerable attention in the early part of this century. Ch'en and Takeo[17] published a comprehensive review of foreign gas effects on spectral lines for astrophysical applications. In their review, theoretical calculations of atomic and molecular collisional interactions were surveyed and compared with existing experimental results. Later, Traving[18] published a review of collisional effects encountered in plasma diagnostics. This area of research experienced rapid growth following the recognition that the influence of collisions on spectral lines provided a means for a noninvasive measurement of local thermodynamic properties.

For iodine in air or nitrogen, the primary collisional interaction arises from dispersive forces. Although I_2, N_2, and O_2 are all nonpolar diatomic molecules, their electron distributions can be influenced in such a way as to induce momentary dipoles and thereby create an intermolecular electronic potential. Iodine, in particular, has a large electron cloud that is easily deformed. The potential resulting from a dispersive interaction is typically written as[18]

$$V(R) = \frac{C_6}{R_{AB}^6} = -\frac{3}{2}\left(\frac{E_{I_A} E_{I_B}}{E_{I_A} + E_{I_B}}\right)\frac{\alpha_A^0\,\alpha_B^0}{(4\pi\epsilon_0)^2}\,\frac{1}{R_{AB}^6}, \tag{1}$$

where E_{I_A} and E_{I_B} are the ionization energies of the interacting molecules, α_A^0 and α_B^0 are their static polarizabilities, R_{AB} is the distance between colliders, and ϵ_0 is the vacuum permittivity. The negative sign indicates that the induced dipole potential is attractive, and only the first term of the interaction potential is considered.

In the derivation of the above relation, it is assumed that the polarizability can be represented by a single-term dispersion formula.[16] Furthermore, it is also assumed that neither colliding species is optically active, so that resonance effects are ignored. This assumption is not valid for the $B \leftarrow X$ system of I_2, which is under investigation here. Therefore, the above representation is not strictly applicable, and any results derived from its use will only be approximate.

Expressions for the collision-induced shift and broadening can be derived for two limiting conditions: the impact limit and the static limit.[15] The former applies to relatively low density situations, where collisions can be treated as independent events and their effects are additive. Static theory is applicable to high densities where multiple collisions can occur simultaneously. When the intermolecular spacing is greater than the Wiesskopf radius,[18] the molecules are far enough apart that impact theory applies. For the dispersive interaction potential that governs iodine-air collisions, the density at which the intermolecular spacing becomes less than the Wiesskopf radius exceeds the range of densities of this work by two orders of magnitude.[20] Consequently, only collisions in the impact limit will be considered in the following analysis.

From Lindholm–Foley collision theory, as given by Traving,[18] the collisional shift in the impact regime expected from the dispersive potential is

$$\Delta\nu_s = \frac{2.94}{2\pi}\,(\Delta C)^{2/5}\langle v^{3/5}\rangle n\left(\frac{\Delta C}{|\Delta C|}\right), \tag{2}$$

where $\Delta\nu_s$ is the frequency shift in GHz. The total number density, n, includes all perturbers, and ΔC is the difference between upper and lower state interaction potential constants for the emitting species, divided by Plancks constant.[15,21] The molecular speed in equation (2) is determined from an average over the Maxwellian distribution of the perturbing molecules.

$$\langle v^{3/5}\rangle = 0.891\langle v\rangle^{3/5},$$

where $\langle v\rangle$ is the mean molecular speed based on temperature and perturber mass,

$$\langle v\rangle = \sqrt{\frac{8kT}{\pi m}}.$$

The final term in Eq. (2) determines the direction of the frequency shift. It is adapted from the Lindholm–Foley formulation of Ch'en and Takeo.[17]

For the dispersion interaction, the difference between the upper and lower state potential constants is

$$\Delta C = \frac{1}{h}(C_{6U} - C_{6L}) = \frac{3}{2h}\left[\left(\frac{E_{I_A}E_{I_B}}{E_{I_A}+E_{I_B}}\right)\left(\frac{\alpha_A^0\alpha_B^0}{(4\pi\epsilon_0)^2}\right)_L - \left(\frac{E_{I_A}E_{I_B}}{E_{I_A}+E_{I_B}}\right)\left(\frac{\alpha_A^0\alpha_B^0}{(4\pi\epsilon_0)^2}\right)_U\right],$$

where the subscripts U and L refer to the upper and lower states, respectively. Let subscript A denote the absorbing iodine molecule whose absorption frequency is being shifted and broadened by colliding molecule B. The perturbing, B, molecules are not participating in the excitation process since they are not resonant with the radiation wavelength. Hence, the expression for the constant can be simplified to

$$\Delta C = \frac{3E_{I_B}}{2h}\frac{\alpha_B^0}{(4\pi\epsilon_0)^2}\left[\frac{E_{I_{AL}}\alpha_{AL}^0}{(E_{I_{AL}}+E_{I_B})} - \frac{E_{I_{AU}}\alpha_{AU}^0}{(E_{I_{AU}}+E_{I_B})}\right]. \tag{3}$$

The difference in interaction potentials for the two I_2 states involved in the absorption process is due to different values of polarizability and ionization energy.

Table 1 contains polarizability and ionization energy values for N_2, O_2, and I_2. There is little information about upper-state polarizabilities for most molecules, due to the difficult task of accounting for the contributions from all of the electronic states.[25] However, the molecular polarizability scales approximately with the molecular volume [26] and the upper state equilibrium spacing, R_e, for I_2 is larger than that of the ground state. This allows an approximate estimate of the upper-state I_2 polarizability,

$$\alpha_{AU}^0 = \left(\frac{R_{eU}}{R_{eL}}\right)^3 \alpha_{AL}^0.$$

For iodine, the upper-state and lower-state equilibrium spacings are 3.016 and 2.666 Å, respectively.[27] Use of these values in the above relation yields a polarizability value that is $\approx 45\%$ greater than that of the lower state. If transfer to other levels of the upper state is neglected, then the upper state ionization energy is effectively the difference between the lower state ionization potential and the energy of the specific transition investigated in this work (at 543 nm this difference is 2.28 eV).

To obtain average air interaction properties, the N_2 and O_2 values were averaged on a mole fraction basis.[28,29] The air polarizability value calculated in this manner, and given in Table 1, matches the value derived from published data for the refractive index of air as a function of wavelength.[24]

Using the interaction parameters given in Table 1, ΔC was determined from Eq. (3). The expected frequency shift due to collisions was then calculated from Eq. (2), along with the ideal gas equation of state, to be

$$\Delta\nu_s = -0.065P/T^{0.7}, \tag{4}$$

where the constant has units of GHz($K^{0.7}$)/torr.

Higher order terms in the dispersion interaction potential scale as R^{-8} and R^{-10}. Using the values from Table 1 in expressions for these terms as given by Margenau,[16] the C_8 and C_{10} magnitudes were calculated to be $<3.6\%$ of the C_6 term for all conditions of this work. It therefore appears reasonable to ignore their contribution to the interaction potential.

One further aspect of the Lindholm–Foley theory is noteworthy. The predicted collisional broadening should have the same thermodynamic scaling as the collisional shift. Moreover, the

Table 1. Static polarizabilities and ionization potentials used in collisional shift calculation.

Molecule	$\alpha/4\pi\epsilon_0$ (Å^3)	E_I(eV)
N_2	1.75[22]	15.576[24]
O_2	1.61[22]	12.063[24]
Air	1.72	14.86
I_{2L}	10.24[23]	9.280[24]
I_{2U}	14.78	7.000

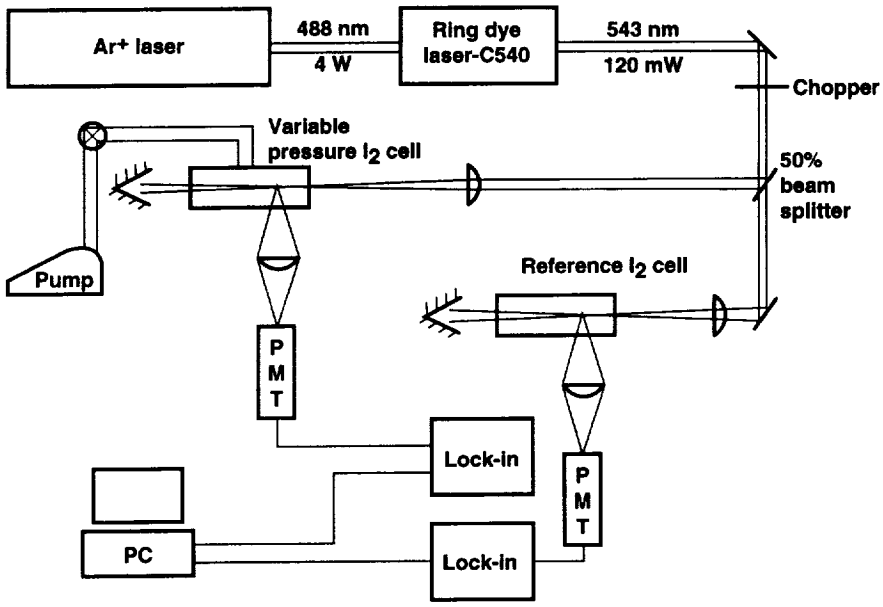

Fig. 1. Optical configuration for the static cell collisional shift measurement experiments.

ratio of broadening to (absolute value of) shift should be a constant that depends only on the interaction potential. For an R^{-6} potential, the expected ratio is 2.75.[18] Therefore, the collisional broadening for I_2 in air should be

$$\Delta\nu_B = 0.179P/T^{0.7}. \tag{5}$$

However, measurements from a large number of molecular systems indicate that, although the ratio of broadening to shift is a constant, no single value is obtained for a particular interaction potential.[17,18]

EXPERIMENTAL CONFIGURATION

Experiments were conducted in both static-cell and jet-flow facilities. The static cell experiments provided a measurement of collisional shift and broadening dependence on the perturber gas (air) pressure at constant temperature conditions. In the flow experiments, the variation in pressure and temperature allowed a determination of the temperature dependence of the collisional shift and broadening, although the flow conditions were less certain than the static cell conditions.

A schematic of the optical configuration used for the static cell experiment is shown in Fig. 1. An 18 W argon ion laser was operated at 488 nm to pump a ring dye laser containing Coumarin 540 dye. A photodiode located within the ring cavity monitored the dye laser output power and an interferometer provided a record of the single mode stability during the 30 GHz dye laser scan. The laser beam was chopped to provide a reference signal for phase-sensitive, lock-in-amplified detection. The beam was then passed through a 50/50 glass beamsplitter to provide equal laser power to the two static cells. The broadband fluorescence emission that resulted from the excitation of the iodine transitions in each cell was collected by a lens and delivered to identical Hamamatsu R2066 PhotoMultiplier Tubes (PMTs) in Pacific Instruments R62/3A14 housings with preamplifiers. For each cell, the collection volume was positioned at the same distance, 8 mm, from the beam entrance to minimize the influence of absorption on the line shapes. Both PMTs were fitted with a multi-layer reflective filter, Bausch & Lomb model 90-2-600, and a long-pass absorbing filter, Hoya Optics 560, to reject scattered laser light. Output signals from the two PMT housings were sent to identical lock-in amplifiers. The amplified signals were digitized by the microcomputer-controlled data acquisition system.

Each cell contained pure I_2 crystals which produced about 0.32 torr vapor pressure of gaseous I_2 at room temperature (293 K). One static cell was sealed to provide a constant, I_2-vapor pressure reference at room temperature. The second static cell was operated at variable pressures by the use of a vacuum pump and valve. The variable cell pressure was measured by an MKS Baratron pressure transducer to an accuracy of $\pm 2\%$ of reading. Temperatures of both cells were monitored to an accuracy of ± 1 K by using thermocouples fastened to the walls. Bottled air was admitted to the variable-pressure cell until the desired pressure was reached. Once the pressure stabilized, a trigger pulse from the microcomputer initiated the ring dye laser scan and 600 discrete fluorescence signal measurements were acquired during the 30 GHz scan.

Because there was no bulk flow of gas within the static cells, the velocity component in the direction of the laser beam was zero; therefore, any shift of the absorption frequency was due to collisions. Excitation spectra obtained from the dye laser scans were normalized for laser intensity variation during the scan using the power monitor reading from the dye laser cavity. Near the peak of each absorption transition the recorded signals were numerically integrated to determine the transition centroid. This was done for the transitions from both cells and the collisional frequency shift was then determined by subtracting the centroid frequency of the variable pressure cell signal from the centroid frequency of the reference cell signal. Since the dye laser scan range varied with temperature, the measured shift was normalized by the distance between the two dominant transitions, which was known.[30] Based on tests with artificially generated spectra and full fits to the line shapes, the measured shifts obtained in this manner have an uncertainty of ± 0.025 GHz.

STATIC CELL RESULTS

Examples of excitation spectra obtained from the two room-temperature static cells are shown in Fig. 2. The variable cell was at a pressure of 348 torr for the measurement shown in this figure. Fluorescence signals are displayed on the figure as a function of the relative dye laser frequency (which corresponds to the direction of increasing absolute frequency) and the two dominant absorption transitions are identified by their rotational and vibrational quantum numbers.[30] The

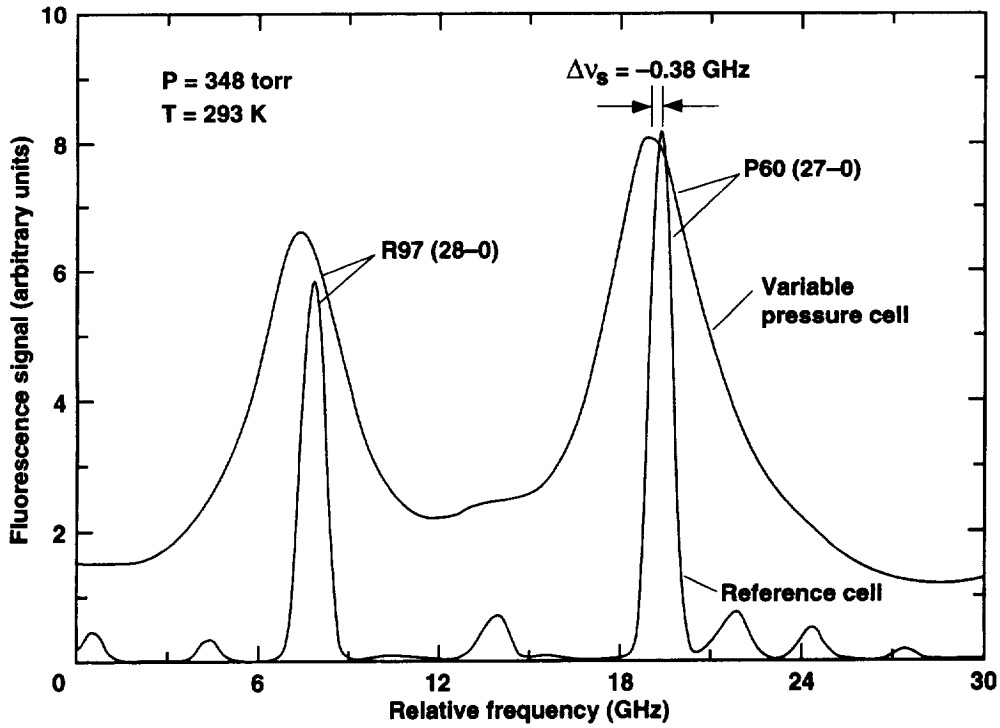

Fig. 2. Excitation spectra of I_2 from the variable-pressure and reference static cells. Note the red-shift and additional broadening of the variable-pressure cell spectrum.

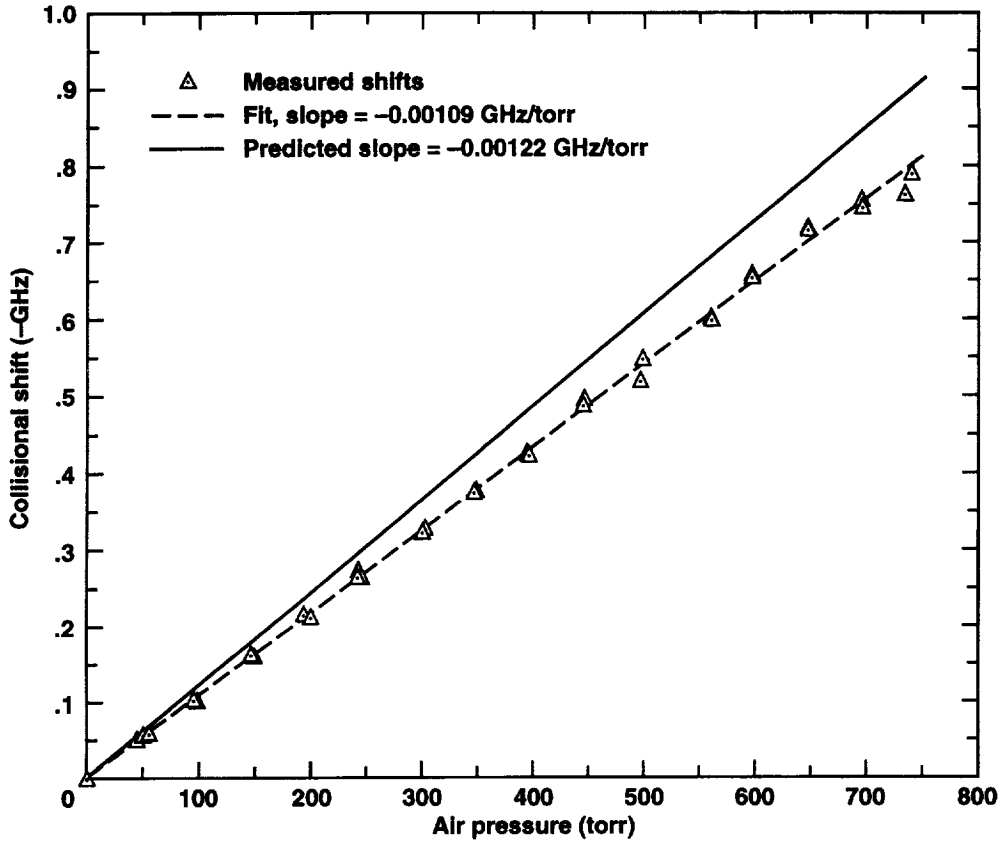

Fig. 3. Collisional shift measurements from the static cell experiment. Note that the predicted slope is 11% greater than the measured slope for the constant temperature experiment.

reference cell spectrum is very sharply resolved, while the spectrum from the variable pressure cell shows additional broadening, due to collisions. Also, the transitions in the variable cell spectrum appear shifted to lower (absolute) frequency than those in the evacuated cell, as predicted by Eq. (4). The measured shift and the recorded experimental thermodynamic conditions are also indicated on the figure.

Collisional shift values derived from similar scans at air pressures ranging from zero to atmospheric are shown in Fig. 3 as a function of air pressure. The measured shifts are to lower absolute frequency (red-shifts) and are plotted in units of ($-$GHz). A linear dependence of the shift on pressure is clearly shown by the distribution of measurements. This confirms the pressure dependence predicted by Eq. (4) for the collisional shift at constant temperature, although the slope of the linear fit to the data (dashed line) does not match the predicted slope (solid line) for variable pressure at a constant temperature of 293 K. Possible explanations for this discrepancy will be discussed in a later section.

FLOWFIELD RESULTS

To evaluate the validity of the predicted temperature scaling of the collisional shift and broadening, experiments were performed using an underexpanded-jet flow. The range of thermodynamic property variation for the jet flow coincided with the intended aerodynamic application range for the LIIF technique.[20]

A schematic representation of the flow is shown in Fig. 4. The underexpanded jet results from the expansion of a dense gas into a low density background.[31-33] A shock system, consisting of a barrel shock and normal shock, encompasses a region of inviscid, expanding core flow. Within this flow region, the expansion is isentropic, and the thermodynamic properties depend only on the

flow Mach number and the reservoir conditions. The location of the normal shock, or Mach disk, is fixed by the ratio of the flow stagnation pressure, P_0, to back pressure, P_b in the enclosure. A converging nozzle is used to accelerate the flow upstream of the sonic nozzle exit, and the choked flow exits from the nozzle into a fused quartz dye laser cell. The jet radius, R_J, is the characteristic dimension of the flowfield and has a value of 1.38 mm. The axial direction, along which measurements of the collisional shift were obtained, is denoted by Z. Also shown in the figure is the propagation direction of the laser beam, normal to the jet flow centerline. As long as the detector aperture observes the jet centerline, where there is no radial velocity component, the measured frequency shifts will only be due to collisions since the flow velocity vector and laser propagation vector are at right angles to each other.

Flow properties at the measurement locations were calculated using typical stagnation conditions and a Mach number distribution that was generated from a numerical solution of the characteristic equations for the flow.[33] Near the orifice exit, where the gas undergoes rapid expansion, the property gradients are very large. Consequently, precise spatial positioning is needed to ensure measurement repeatability and accurate knowledge of thermodynamic conditions.

The configuration was changed from the static cell experiments by the substitution of the jet for the variable-pressure cell. Bottled air was used to supply the jet and the flow stagnation pressure and temperature, T_0, were monitored during the runs. Instead of recording broadband fluorescence from a static cell, the second PMT recorded the signal from within the underexpanded jet flowfield. In contrast to the static cell experiments, I_2 was seeded into the airflow in a large-volume, constant-temperature mixing vessel located upstream of the convergent jet nozzle. A microcomputer-controlled, stepper-motor-driven translation system was used to position the PMT observation point along the jet centerline. The laser beam was brought to the jet flow by five stage-mounted mirrors which maintained fixed laser beam pointing relative to the PMT collection aperture. A 135 mm focal length lens provided a 35 μm diameter beam at the jet centerline, a value which was $<3\%$ of the jet radius. Combined with a collection aperture height of 100 μm, the narrow beam waist provided sufficient resolution of the large-gradient region of the flow. Centering of the observation point in the jet was achieved by positioning the PMT at the midpoint of the distance between lateral locations of the barrel shock, where equivalent

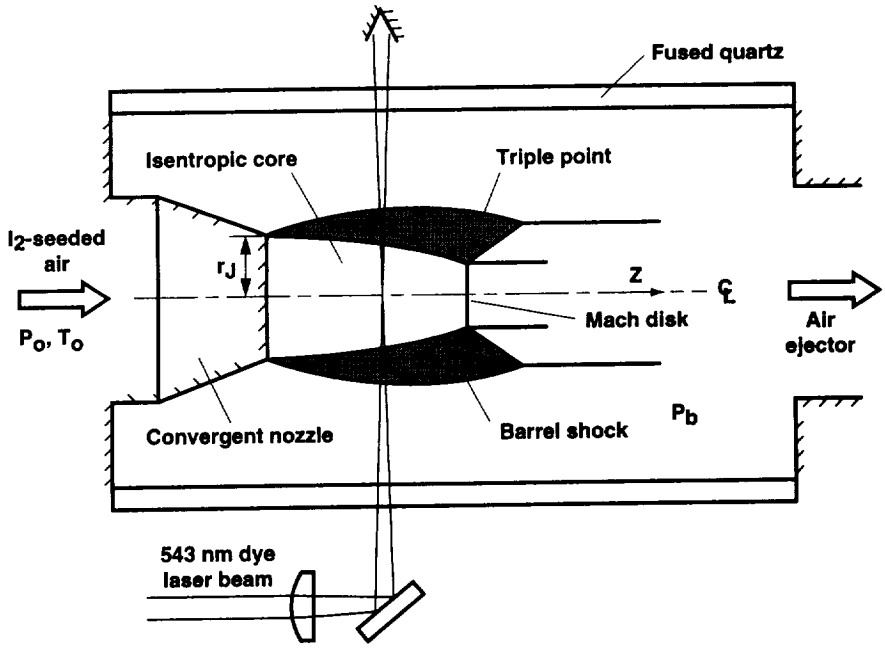

Fig. 4. Underexpanded jet flowfield and optical configuration. Measurements were made along the jet centerline.

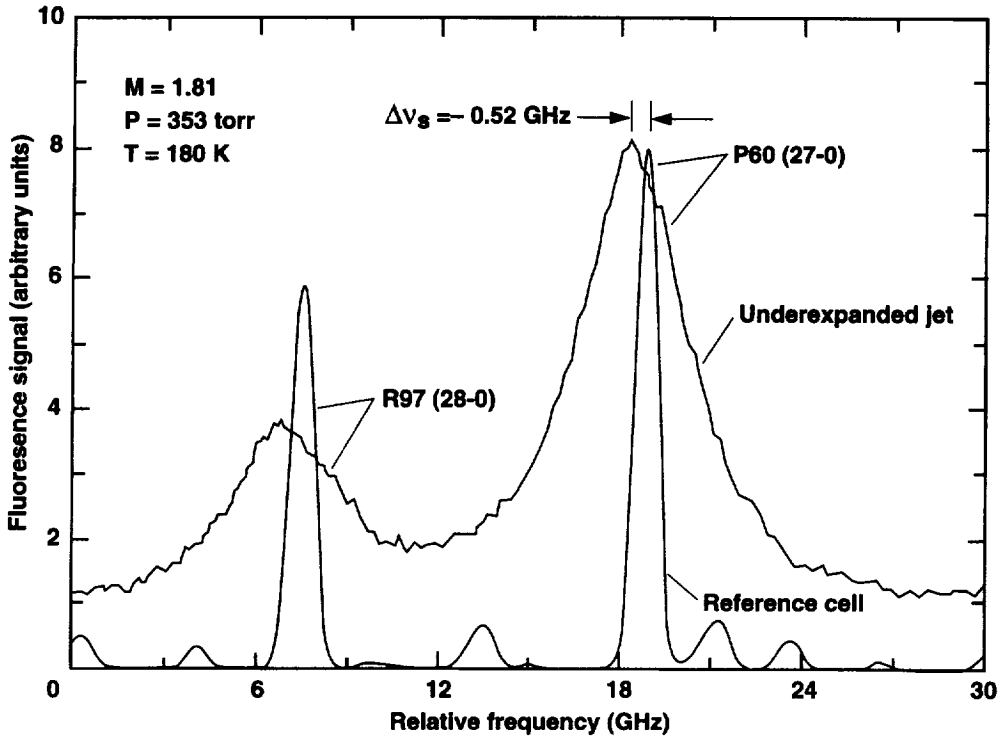

Fig. 5. Excitation spectra of I_2 from the underexpanded-jet flow and reference cell. Note the increased red-shift relative to that of Fig. 2 due to the reduced temperature.

fluorescence signal values were encountered. The data acquisition procedure was essentially unchanged from the static cell experiments.

Excitation spectra from the underexpanded jet experiment are shown in Fig. 5. In the figure, the more sharply peaked spectrum is from the reference cell and the broader spectrum is the fluorescence signal from the flow location. At this location, the flowfield static pressure is 353 torr, which closely matches the variable cell pressure for the spectra presented in Fig. 2. However, since the flow cools as it expands, the flow-static temperature at this location is 180 K, considerably lower than room temperature. The effect of lower temperature on the spectrum is illustrated by comparing the signal level of the first transition in Fig. 5 to that of Fig. 2. The decreased signal level of the $R97(28–0)$ transition is due to its reduced Boltzmann population at 180 K. The collisional shift measured at this location is indicated in the figure. It is greater than the shift measured at the same pressure in the static cell experiment (see Fig. 2), due to the decreased temperature.

Results from similar measurements at all flow locations from three different tests are shown in Fig. 6. The negative frequency shift measured at each location is plotted as a function of $P/T^{0.7}$. A log–log plot is used instead of a linear plot to avoid obscuring the very small shifts measured in the highly expanded flow regions. Although it is not strongly evident on the log–log plot, there is more scatter in the flowfield shift measurements when they are compared with the static cell results. This is primarily due to the greater uncertainty in the flowfield thermodynamic parameters, especially near the nozzle exit. This uncertainty is approx. 5.8% of the local value of $P/T^{0.7}$. The dashed line through the measurements represents the least-squares fit slope (-0.058 GHz $K^{0.7}$/torr) that was derived from the static cell measurements of Fig. 3. The uncertainty in the slope derived from all of the measurements, which represents the collisional shift constant for I_2 in air at 543 nm, is ± 0.004 GHz $K^{0.7}$/torr. From both experiments the measured slope is within 11% of the theoretically predicted value, -0.065 GHz $K^{0.7}$/torr. The agreement between the shift measurements from the flow and static cell indicates that the temperature scaling predicted by the collisional impact theory is correct.

COLLISIONAL BROADENING MEASUREMENT AND RESULTS

A study of the collisional broadening was also performed using the experimental data from the underexpanded-jet flowfield. While it is not immediately apparent from the spectral distribution of Fig. 2, the fluorescence signals from the two transitions contain significant contributions from adjacent transitions, even at the transition centers. Therefore, a determination of the collisional broadening at this condition must account for these adjacent-line contributions,[5,6] which must be properly weighted by their relative absorption strengths. The collisional shift is less sensitive to the fluorescence signal contributions from adjacent lines since the distribution of neighboring transitions is relatively symmetric for the two transitions shown.[30] For this reason, the collisional shift measurements were used to determine the validity of the $P/T^{0.7}$ thermodynamic scaling of the collisional processes predicted by Eqs. (4) and (5). A numerical model of the excitation process,[20] which included this scaling for collisional broadening, was then used to calculate the spectral distribution and account for the neighboring transition contributions. Using different values of the collisional broadening constant in Eq. (5), the spectral distribution was calculated at each measurement condition and compared with the measured spectrum to determine the best value of the constant. This procedure resulted in a best-fit collisional broadening constant at each thermodynamic condition in the jet flow.

The numerical model of the laser-excitation process summed all of the more strongly populated transitions within 60 GHz of the transitions of interest. Spectral positions of the transitions were derived from the Iodine Atlas of Gerstenkorn and Luc[30] and the transition strengths were calculated using the Franck–Condon factors and R-Centroid values tabulated by Tellinghuisen.[34] The model treats each transition as single line with a fixed contribution to the total linewidth to represent the

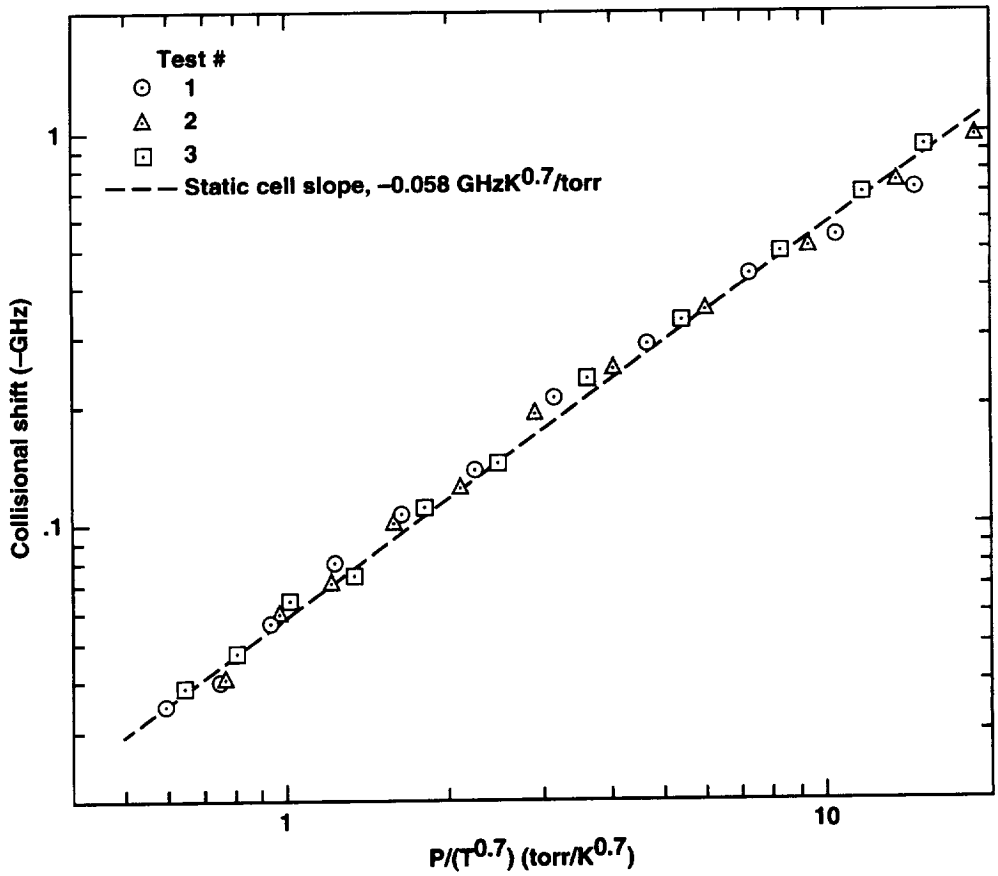

Fig. 6. Collisional shift measurement results from the underexpanded-jet flow experiment. The dashed line is the slope of the linear least-squares fit to the static cell measurements of Fig. 3.

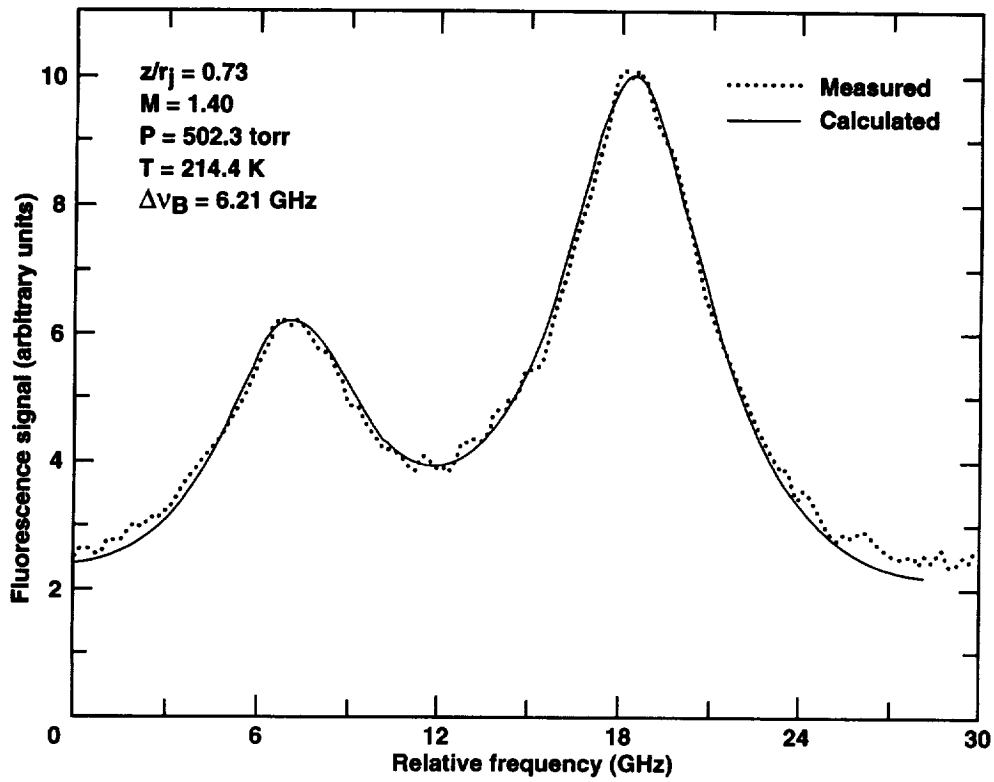

Fig. 7. Comparison of calculated and measured excitation spectra for the underexpanded-jet flow. The spectral calculation treated each transition as a single line with a fixed hyperfine broadening contribution.

effect of hyperfine splitting. This contribution is added to the Doppler width to give a total inhomogeneous full-width-at-half-maximum (FWHM) of

$$\Delta\nu_D = \sqrt{\frac{8(\ln 2)kT}{mc^2}}\,\nu_0 + \Delta\nu_{hf},$$

where T is the local temperature and $\Delta\nu_{hf}$ is the hyperfine linewidth (0.352 GHz).[35] The inhomogenous broadening contribution is then convolved with the collisional broadening using a Voigt line shape representation. This model of the transitions was reasonably accurate to $P/T^{0.7} = 2.45$ torr/K$^{0.7}$. Below this value, the collisional broadening becomes small enough that the model seriously underpredicts the linewidth since the hyperfine transition distribution is not modeled.

This was remedied at the low pressure and temperature conditions by modelling the hyperfine splitting using the approximate expression for large values of rotational quantum number given by Levenson and Schawlow.[36] The model included the hyperfine splitting contributions from both the nuclear-electric quadruple coupling and magnetic spin–rotation interaction. The actual interaction constants for the I_2 transitions of interest were calculated using the formulas given by Gläser.[37] There are 21 hyperfine levels for transitions with odd values of the ground state rotational quantum number and 15 hyperfine levels for even values. Each of the hyperfine transitions was modeled with a Voigt line shape and a natural linewidth of 80 MHz.

Examples of the numerical fits to the measured excitation spectra are shown in Figs. 7 and 8. The thermodynamic conditions at the respective measurement locations are indicated. The calculated spectral distribution in Fig. 7 is obtained from the single-transition representation with a constant hyperfine width contribution. In Fig. 8, for the lower pressure condition, the spectrum is calculated using the resolved hyperfine components of each transition. Results from these fits at all measurement locations gave values of the collisional width for each measurement. These

values are plotted vs $P/T^{0.7}$ in Fig. 9. The slope of a linear fit to the measurements, which was constrained to pass through zero, is 0.531 GHz $K^{0.7}$/torr. The uncertainty in the measured slope, which represents the collisional broadening constant for I_2 in air at 543 nm, is ± 0.009 GHz $K^{0.7}$/torr. The larger value for the uncertainty in the collisional broadening measurements represents the cumulative effect of the uncertainties in all of the contributions to the measured transition widths. The ratio of measured collisional broadening to shift is 9.16, considerably greater than the theoretical ratio of 2.75.

DISCUSSION OF EXPERIMENTAL RESULTS

The difference between the predicted and experimentally-derived slopes for the collisional shift is most likely due to inaccuracies in the calculated interaction constant, ΔC, which was derived from average I_2 and air properties. The use of a nonresonant polarizability for I_2 and single-term dispersion representations for both species, while useful for simplifying the analysis, are not strictly justified. Moreover, the polarizability value for the I_2 upper state is a recognized approximation. An accurate, quantum mechanical calculation of the upper state polarizability at 543 nm[25] would very likely improve the comparison between measurements and theory.

The experimental results also indicate that the collisional shift does not change drastically over the 30 GHz measurement range. Both of the stronger transitions, $P60(27\text{–}0)$ and $R97(28\text{–}0)$ appear to shift equally with pressure and temperature. Despite the large difference in rotational quantum number, an average polarizability value appears to be an adequate representation of the collisional activity; however, the results in this wavelength region are not expected to apply to all wavelengths within the $B\text{–}X$ system, since the upper state polarizability value can have wide variation.[38]

For the flow measurements, the I_2 seeding fraction is estimated to be between 150 and 200 parts-per-million (ppm), while for the static cell measurements the seeding fraction ranged from

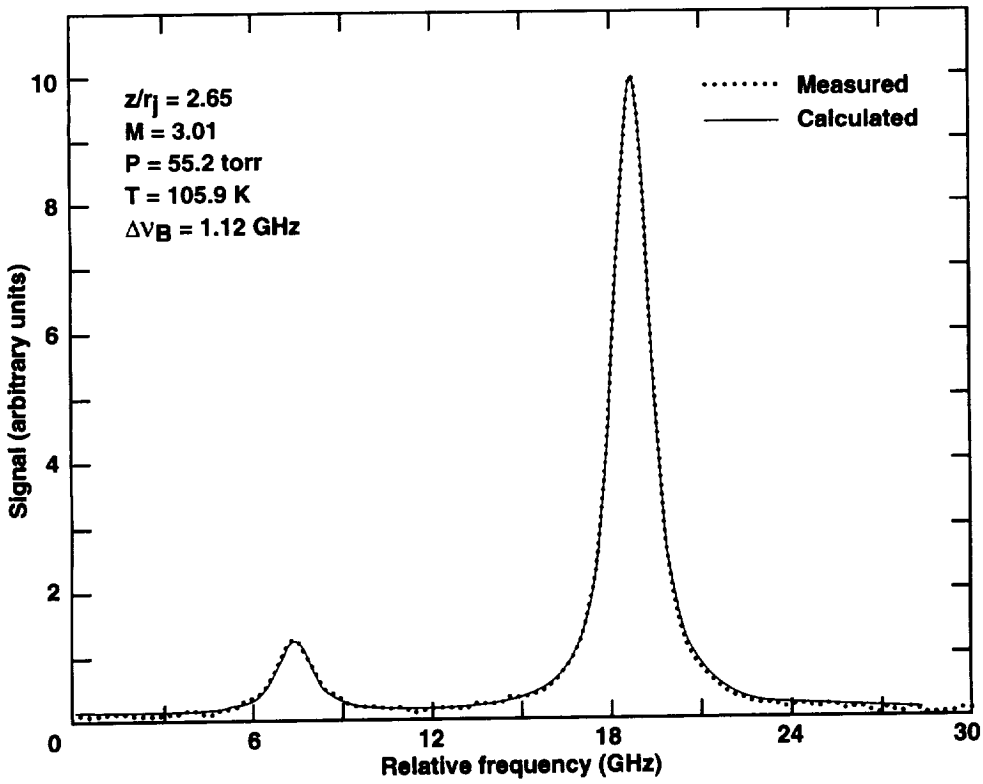

Fig. 8. Comparison of calculated and measured excitation spectra for the underexpanded-jet flow. The spectral calculation modeled each hyperfine transition separately.

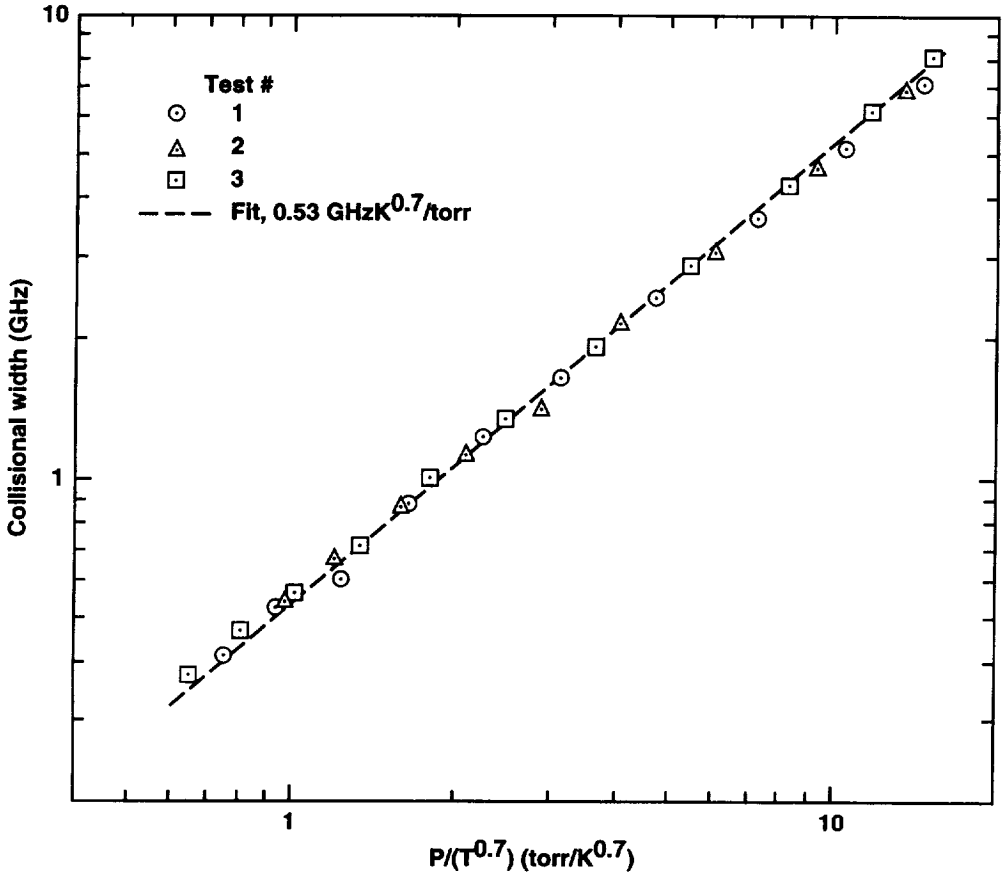

Fig. 9. Collisional broadening measurement results from the underexpanded-jet flow experiment. The dashed line is a linear least-squares fit to the measurements that is constrained to pass through zero.

430 to 10^6 ppm. From the distribution of collisional shift measurements, there does not appear to be a strong dependence on I_2 seeding fraction. However, the collisional shift measurements are made relative to the line position in a 0.32 torr I_2 cell, so any contribution from I_2–I_2 collisions at that vapor pressure will be subtracted off for both static cells. Still, over the range of measurements, it appears that the dominant potential interaction is due to the more probable I_2–air collisions.

It is conceivable that repulsive interactions occur at higher densities to counteract the red shift of the attractive dispersion interaction. At the highest pressures of this study, the transition center locations become less certain as the signal contributions from adjacent-line broadening begin to overwhelm the initial transition signal; therefore, the possibility of a repulsive interaction must be investigated with a more isolated absorption transition.

The measured scalings of the collisional shift and broadening with temperature contradict the scaling reported by Hiller and Hanson in their review of I_2 properties for aerodynamic measurement applications.[39] Apparently, they assumed that the collisional shift and broadening scaled as $P/T^{0.5}$. The $T^{-0.5}$ scaling is encountered in Lorentzian theory; however, as discussed by Ch'en and Takeo,[17] Lorentzian theory does not predict a collisional shift, since it does not account for phase-interrupting collisions. The value given for the collisional shift, 0.0242 GHz $K^{0.5}$/torr, in Ref. 39 is also incorrect.

CONCLUSIONS

The thermodynamic scaling of the collisional shift and broadening of I_2 spectral lines in air was investigated. Measurements of shift and broadening were obtained from static cell and underexpanded-jet flow experiments. The static cell tests provided high resolution measurements of the shift

as a function of pressure, and the flow experiments provided a means for additionally measuring the temperature dependence of the collisional shift. Calculations of the collisional shift using Lindholm–Foley theory for a dispersive interactive in the impact limit agreed reasonably well with the experimental measurements, despite the questionable assumptions about the applicable I_2 polarizabilities. The largest source of uncertainty in the calculated shift is believed to be the approximation of the upper-state molecular polarizability. The calculated value of the upper state I_2 polarizability is not reliable since it was estimated without accounting for contributions from other I_2 electronic states.

As predicted by the theory, the thermodynamic scaling of collisional broadening was found to be identical to that of the collisional shift; however, the experimentally determined ratio of broadening to shift did not match the theoretical value. This observation regarding the ratio is in agreement with results from previous experiments for dispersion interactions.

Acknowledgements—This work was supported by NASA grant NAG-1-373, Dr. G. Burton Northam, technical monitor. The excellent work of Roy Hartfield on the jet nozzle fabrication is gratefully acknowledged.

REFERENCES

1. R. L. McKenzie, *AIAA J.* **31,** 465 (1993).
2. A. Y. Chang and R. K. Hanson, *JQSRT* **42,** 207 (1989).
3. G. A. Raiche and D. R. Crosley, *J. Chem. Phys.* **92,** 5211 (1990).
4. J. C. McDaniel, "Quantitative measurement of density and velocity in compressible flows using laser-induced iodine fluorescence", AIAA Paper No. 83-0049 (1983).
5. J. C. McDaniel, *Prog. Astron. Aeronaut.* **92,** 107 (1984).
6. D. G. Fletcher and J. C. McDaniel, *Opt. Lett.* **12,** 16 (1987).
7. B. Hiller and R. K. Hanson, *Appl. Opt.* **27,** 33 (1988).
8. D. G. Fletcher and J. C. McDaniel, *AIAA J.* **27,** 575 (1989).
9. T. Ni-Imi, T. Fujimoto, and N. Shimizu, *Opt. Lett.* **15,** 918 (1990).
10. R. J. Hartfield, S. Hollo, and J. C. McDaniel, *AIAA J.* **31,** 483 (1993).
11. J. M. Donahue, J. C. McDaniel, and H. Haj-Hariri, *AIAA J.* **32,** 1860 (1994).
12. R. B. Miles, W. R. Lempert, and J. N. Forkey, "Instantaneous velocity fields and background suppression by filtered Rayleigh scattering", AIAA Paper No. 91-0357 (1991).
13. H. Komine and S. J. Brosnan, *Laser Anemometry* **1,** 273 (1991).
14. G. S. Elliott, M. Samimy, and S. A. Arnette, "Molecular filter-based diagnostics in high speed flows", AIAA Paper No. 93-0512 (1993).
15. H. Margenau and W. W. Watson, *Rev. Modern Phys.* **8,** 22 (1936).
16. H. Margenau, *Rev. Modern Phys.* **11,** 1 (1939).
17. S. Ch'en and M. Takeo, *Rev. Modern Phys.* **29,** 20 (1957).
18. G. Traving, "Interpretation of line broadening and line shift", in *Plasma Dynamics*, W. Lochte-Holtgreven, ed., p. 66, North-Holland, Amsterdam (1978).
19. J. O. Hirschfelder, C. F. Curtiss, and R. B. Byrd, *Molecular Theory of Gases and Liquids*, p. 963, Wiley, New York (1954).
20. D. G. Fletcher, "Spatially-resolved, nonintrusive measurements in a nonreacting scramjet combustor using laser-induced iodine fluorescence", Ph.D. dissertation, Dept. of Mech. and Aero. Engr., Univ. of Virginia, Charlottesville (1989).
21. H. M. Foley, *Phys. Rev.* **69,** 616 (1946).
22. K. M. Swift, L. A. Schlie, and R. D. Rathge, *Appl. Opt.* **27,** 4381 (1988).
23. G. Maroulis and A. J. Thakkar, *Molec. Phys.* **73,** 1235 (1991).
24. R. C. Weast, ed., *CRC Handbook of Chemistry and Physics*, 62nd ed., pp. (E)72–76. CRC Press, Boca Raton (1981).
25. R. E. Johnson, *Introduction to Atomic and Molecular Collisions*, p. 120, Plenum Press, New York (1982).
26. G. W. Castellan, *Physical Chemistry*, 3rd ed., p. 644, Addison-Wesley, Reading, MA (1983).
27. G. Herzberg, *Molecular Spectra and Molecular Structure I. Spectra of Diatomic Molecules*, 2nd ed., Van Nostrand, New York, p. 541 (1951).
28. B. Folkesson and R. Larsson, *Journal of Electron Spectroscopy and Related Phenomena*, **50,** p. 251 (1990).
29. M. Born and E. Wolf, *Principles of Optics* 4th ed., p. 89, Pergamon Press, Oxford (1970).
30. S. Gerstenkorn and P. Luc, "Atlas du spectre d'absorption de la molecule d'lode, complement", Centre National de la Recherche Scientifique, Paris (1986).
31. H. Ashkenas and F. S. Sherman, in *Rarefied Gas Dynamics*, Vol. 2, p. 84, Academic Press, New York (1966).
32. H. R. Murphy and D. R. Miller, *J. Chem. Phys.* **88,** 4474 (1984).
33. E. K. Gustafson, Private communication, Dept. of Applied Physics, Stanford Univ, Stanford, CA.
34. J. Tellinghuisen, *JQSRT* **19,** 149 (1978).

35. S. Gerstenkorn, P. Luc, and R. Vetter, *Rev. Phys. Appl.* **16,** 529 (1981).
36. M. D. Levenson and A. L. Schawlow, *Phys. Rev. A* **6,** 6 (1972).
37. M. Gläser, *Opt. Commun.* **54,** 335 (1985).
38. W. Huo, Private communication, Computational Chemistry Branch, MS 230-3, NASA Ames Research Ctr., Moffett Field, CA.
39. B. Hiller and R. K. Hanson, *Exp. Fluids* **10,** 8 (1990).